SCIENCE CHINA
Physics, Mechanics & Astronomy

• Article •

March 2020 Vol. 63 No. 3: 230411
https://doi.org/10.1007/s11433-019-9604-x

Holographic p-wave superfluid with Weyl corrections

YongHao Huang[1], QiYuan Pan[1,2*], Wei-Liang Qian[2,3,4], JiLiang Jing[1,2], and ShiLiang Wang[5]

[1] *Key Laboratory of Low Dimensional Quantum Structures and Quantum Control of Ministry of Education, Synergetic Innovation Center for Quantum Effects and Applications, and Department of Physics, Hunan Normal University, Changsha 410081, China;*
[2] *Center for Gravitation and Cosmology, College of Physical Science and Technology, Yangzhou University, Yangzhou 225009, China;*
[3] *Escola de Engenharia de Lorena, Universidade de São Paulo, Lorena 12602-810, Brazil;*
[4] *Faculdade de Engenharia de Guaratinguetá, Universidade Estadual Paulista, Guaratinguetá 12516-410, Brazil;*
[5] *School of Physics and Electronics, Central South University, Changsha 410083, China*

Received June 12, 2019; accepted July 30, 2019; published online November 25, 2019

In this work, we study the effects of the Weyl corrections on the p-wave superfluid phase transition in terms of an Einstein-Maxwell theory coupled to a complex vector field. In the probe limit, it is observed that the phase structure is significantly modified owing to the presence of the higher order Weyl corrections. The latter, in general, facilitates the emergence of the superfluid phase as the condensate increases with the Weyl coupling measured by γ. Moreover, several features about the phase structure of the holographic superfluid are carefully investigated. In a specific region, the phase transition from the normal phase to the superfluid phase is identified to be the first order, instead of being the second order, as in the cases for many holographic superconductors. By carrying out a numerical scan of model parameters, the boundary dividing these two types of transitions is located and shown to be rather sensitive to the strength of Weyl coupling. Also, a feature known as "Cave of Winds", associated with the emergence of a second superfluid phase, is observed for specific choices of model parameters. However, it becomes less prominent and eventually disappears as γ increases. Furthermore, for temperature in the vicinity of the critical one for vanishing superfluid velocity, denoted by T_0, the supercurrent is found to be independent of the Weyl coupling. The calculated ratio, of the condensate with vanishing superfluid velocity to that with maximal superfluid velocity, is in good agreement with that predicted by Ginzburg-Landau theory. While compared with the impact on the phase structure owing to the higher curvature corrections, the findings in our present study demonstrate entirely different characteristics. Further implications are discussed.

AdS/CFT correspondence, Weyl corrections, holographic superfluid

PACS number(s): 11.25.Tq, 04.70.Bw, 74.20.-z

Citation: Y. H. Huang, Q. Y. Pan, W.-L. Qian, J. L. Jing, and S. L. Wang, Holographic p-wave superfluid with Weyl corrections, Sci. China-Phys. Mech. Astron. **63**, 230411 (2020), https://doi.org/10.1007/s11433-019-9604-x

1 Introduction

The discovery of the high-temperature superconductor by Bednorz and Müller [1] in 1986 marks significant breakthrough in ceramic materials. Despite intense efforts made in recent years, up to date the question of how superconductivity arises in such materials still poses a challenge in theoretical physics. As one of the major unsolved problems, it is understood to be associated with the strong interaction between electron and phonon which cannot be explained by the usual Bardeen-Cooper-Schrieffer (BCS) theory [2]. Anti-de Sitter/conformal field theories (AdS/CFT) correspondence [3-5], on the other hand, provides a possibility to describe a quantum field theory with strong interaction on the boundary in terms of a weakly coupled gravity theory in the bulk. It potentially opens up new avenues for

*Corresponding author (email: panqiyuan@126.com)

understanding the pairing mechanism in the high T_c superconductors [6]. In fact, since the superconductivity is a phenomenon belonging to the field theory, it is quite natural to ask whether the gauge/gravity duality may be used to provide meaningful insights into the problem. As it turns out, there does exist a gravitational dual which closely mimics the properties of a superconductor. To be specific, the spontaneous breaking of the $U(1)$ gauge symmetry of the gravitational theory in the bulk, can be interpreted as the condensate related to the phase transition from a normal state to the superconducting one in the dual system on the boundary [7]. Subsequently, a model for s-wave superconductor was successfully proposed [8]. The resulting system associated with its gravitational dual is hence known as a holographic superconductor [9-12]. Along this line of thought, the holographic p-wave superconductivity was realized by introducing an $SU(2)$ Yang-Mills field into the bulk [13]. Alternatively, the holographic d-wave superconductor can be constructed in terms of the condensate of a charged massive spin two field propagating in the bulk [14, 15]. It is noted that the studies mentioned above focus on the setup where the spatial components of the gauge field vanish. It is the presence of the time component of the vector potential that modifies the effective mass of the relevant field, which consequently leads to the formation of hairs for the black hole. Furthermore, by introducing the spatial component of the gauge field, the authors of refs. [16, 17] constructed a holographic superfluid solution in the AdS black hole background. In this scenario, the superfluid state corresponds to a deformation of superconducting one by turning on the time-independent supercurrent in terms of the spatial component of the gauge field. The latter was found to be essential in determining the order of the superfluid phase transition. On the other hand, in the AdS soliton background, it was found that the first-order phase transition does not take place. In the probe limit, the resulting holographic superfluid phase transition is shown to be always of the second order [18, 19]. Besides the topic related to the specific properties of the phase transition, gravity theories with dual superfluid counterparts are interesting in themselves, owing to their potential applications in condensed matter physics [20-27].

In this work, we focus on a new holographic p-wave model where a charged vector field is introduced into the Einstein-Maxwell theory with a negative cosmological constant [28]. The present approach can be viewed as a generalization of the $SU(2)$ model with a general mass and gyromagnetic ratio proposed in ref. [29]. In the probe limit, it was shown that the instability of the black hole metric leads to the condensate of the vector field, and the latter can be utilized to describe the superconducting phase. In particular, an applied magnetic field may induce the condensate even without any charge density. When one takes the backreaction into account, this p-wave model in question displays a rich phase structure, which includes zeroth-order, first-order and second-order phase transitions [29-32]. In another work [33], based on the Einstein-Maxwell theory coupled to a complex vector field, the phase transition of a holographic superfluid was investigated by introducing the spatial component of the gauge field. The authors observed a turning point where the second-order phase transition becomes a first-order one. The above turning point regarding superfluid velocity was found to be increasing with the squared mass of the vector field. Besides, a feature called "Cave of Winds" was observed in five-dimensional spacetime [20, 34]. It was named after the peculiar shape of the corresponding condensate curve, and physically indicates the emergence of a second superconducting phase. However, it is interesting to note that the Cave of Winds also appears for a certain range of the Lifshitz parameter in the four-dimensional spacetime [35]. The studies have also been extended to the case of bulk AdS soliton background. It was found that the spatial component of the gauge field will hinder the holographic p-wave superfluid phase transitions but does not change the order of the phase transitions [36], even in the presence of dark matter [37].

All the studies mentioned above concerning the holographic p-wave models are mainly based on the Einstein-Maxwell theory coupled to a charged vector field. According to the AdS/CFT correspondence, the higher derivative corrections to either gravitational or electromagnetic part of the action in AdS space are expected to modify the dynamics of the dual strongly coupled theory. More recently, the holographic p-wave superfluid in Gauss-Bonnet gravity was investigated via a Maxwell complex vector field model. In particular, the effect of the curvature corrections on the superfluid phase transition was investigated in the probe limit [38]. It was shown that the higher curvature corrections hinder the condensate of the vector field. On the other hand, the corrections make it easier for the appearance of the turning point where the second-order transition switches to a first-order one as well as for the emergence of the Cave of Winds. The latter indicates that the Gauss-Bonnet parameter may change the order of the phase transition in the dual system. In order to systematically study the effect of the $1/N$ or $1/\lambda$ (with λ being the 't Hooft coupling) corrections on the holographic dual models, it is meaningful to consider the Weyl corrections. This is carried out by coupling the gauge field with the Weyl tensor, which was known to describe a type of gravitational distortion in the spacetime [39, 40]. In ref. [41], the authors introduced a holographic s-wave superconductor model with Weyl corrections. They found that the higher Weyl corrections facilitate condensate of the scalar field. By generalizing the study to the p-wave superconductors, we observed

that the higher Weyl corrections make it easier for the p-wave metal/superconductor phase transition to be triggered [42]. Thus the effects of Weyl corrections in the s-wave and p-wave cases are similar. More recently, there has been an increasing interest in the Weyl corrections regarding the studies of holographic superconductors [43-56].

The present study aims to examine the influence of the Weyl corrections on the holographic p-wave superfluid model. In comparison with our recent work [38], we also analyze our model regarding that with higher order curvature corrections. We understand such comparison might shed light on the effect of the $1/N$ or $1/\lambda$ corrections on the holographic p-wave superfluid models. In fact, while extending the model of holographic p-wave superconductor [42] to study the holographic p-wave superfluid, one finds significant implications. As discussed below in the text, even in the probe limit, where the backreaction of matter fields on the metric is neglected, the Weyl corrections lead to a rich phase structure for the p-wave superfluid. The resulting impact to the model is strong in contrast to that on the p-wave superconductor investigated previously [42]. Moreover, comparisons are also carried out for the effect of the Weyl corrections with that of the higher order curvature corrections, another well-known class of the bottom-up holographic models regarding higher derivatives. The results turn out to be entirely different for these two different classes of higher-derivative corrections.

2 Einstein-Maxwell-complex vector model with Weyl corrections

We start with the action of the Einstein-Maxwell-complex vector model with the Weyl corrections

$$S = \frac{1}{16\pi G}\int \mathrm{d}^5x\sqrt{-g}\left[-\frac{1}{4}\left(F_{\mu\nu}F^{\mu\nu}-4\gamma C^{\mu\nu\rho\sigma}F_{\mu\nu}F_{\rho\sigma}\right) -\frac{1}{2}\rho^{\dagger}_{\mu\nu}\rho^{\mu\nu}-m^2\rho^{\dagger}_{\mu}\rho^{\mu}\right], \tag{1}$$

where $C^{\mu\nu\rho\sigma}$ denotes the Weyl tensor, and the Weyl coupling γ falls within the range of $-1/16 < \gamma < 1/24$ [39]. $F_{\mu\nu} = \nabla_\mu A_\nu - \nabla_\nu A_\mu$ is the Maxwell field strength. The tensor $\rho_{\mu\nu} = D_\mu\rho_\nu - D_\nu\rho_\mu$ with $D_\mu = \nabla_\mu - \mathrm{i}qA_\mu$ being the covariant derivative, and m and q are the mass and charge of the vector field ρ_μ. It should be noted that we will only consider the case without an external magnetic field in this work. Thus, comparing with the action in ref. [42], in the action (1) we have deleted the term $\mathrm{i}q\gamma_0\rho_\mu\rho^{\dagger}_\nu F^{\mu\nu}$, which describes the interaction between the vector field ρ_μ and the gauge field A_μ, since it will not play a part in the present study.

In order to investigate the black hole solution regarding the holographic p-wave superfluid, we consider the following five-dimensional planar Schwarzschild-AdS background metric

$$\mathrm{d}s^2 = -f(r)\,\mathrm{d}t^2 + \frac{1}{f(r)}\mathrm{d}r^2 + r^2\left(\mathrm{d}x^2+\mathrm{d}y^2+\mathrm{d}z^2\right). \tag{2}$$

Subsequently, the nonzero components of the Weyl tensor $C_{\mu\nu\rho\sigma}$ are

$$\begin{aligned} &C_{0i0j} = \frac{r_+^4 f(r)}{r^2}\delta_{ij}, \quad C_{0r0r} = -\frac{3r_+^4}{r^4}, \\ &C_{irjr} = -\frac{r_+^4}{r^2 f(r)}\delta_{ij}, \quad C_{ijkl} = r_+^4\delta_{ik}\delta_{jl}, \end{aligned} \tag{3}$$

where $i,\ j,\ k,\ l = x,\ y$ or z and $f(r) = r^2\left(1-r_+^4/r^4\right)$ with r_+ being the radius of the event horizon. Obviously, the Hawking temperature of this black hole is $T = r_+/\pi$, which is interpreted as the temperature in the dual system.

To derive the equations of motion in the probe limit, we ignore the backreaction of matter fields on the spacetime metric, and vary the action (1) with respect to the vector field ρ_μ and the gauge field A_μ. One finds

$$D^\nu\rho_{\nu\mu} - m^2\rho_\mu = 0, \tag{4}$$

$$\nabla^\nu(F_{\nu\mu} - 4\gamma C_{\nu\mu\rho\sigma}F^{\rho\sigma}) - \mathrm{i}q(\rho^\nu\rho^{\dagger}_{\nu\mu} - \rho^{\nu\dagger}\rho_{\nu\mu}) = 0. \tag{5}$$

In order to investigate the possibility of DC supercurrent, we assume the following ansatz:

$$\rho_\mu\mathrm{d}x^\mu = \rho_x(r)\mathrm{d}x, \quad A_\mu\mathrm{d}x^\mu = A_t(r)\mathrm{d}t + A_y(r)\mathrm{d}y, \tag{6}$$

which subsequently leads to

$$\rho_x'' + \left(\frac{1}{r}+\frac{f'}{f}\right)\rho_x' - \frac{1}{f}\left(m^2 + \frac{q^2A_y^2}{r^2} - \frac{q^2A_t^2}{f}\right)\rho_x = 0, \tag{7}$$

$$\left(1-\frac{24\gamma r_+^4}{r^4}\right)A_t'' + \frac{3}{r}\left(1+\frac{8\gamma r_+^4}{r^4}\right)A_t' - \frac{2q^2\rho_x^2}{r^2 f}A_t = 0, \tag{8}$$

$$\left(1+\frac{8\gamma r_+^4}{r^4}\right)A_y'' + \left[\frac{1}{r}\left(1-\frac{24\gamma r_+^4}{r^4}\right) + \frac{f'}{f}\left(1+\frac{8\gamma r_+^4}{r^4}\right)\right]A_y' - \frac{2q^2\rho_x^2}{r^2 f}A_y = 0, \tag{9}$$

where the prime denotes the derivative with respect to r. Obviously, when the spatial component A_y is turned off, eqs. (7) and (8) fall back to the case considered in ref. [42] for the holographic p-wave superconductor.

By imposing the appropriate boundary conditions, we can solve eqs. (7)-(9) numerically by carrying out an integration from the horizon to the infinity [6]. At the horizon $r = r_+$, the regular conditions are assumed, which implies that all the relevant physical quantities are finite. Near the boundary $r \to \infty$, one obtains the following asymptotic behaviors:

$$\rho_x = \frac{\rho_{x-}}{r^{\Delta_-}} + \frac{\rho_{x+}}{r^{\Delta_+}}, \quad A_t = \mu - \frac{\rho}{r^2}, \quad A_y = S_y - \frac{J_y}{r^2}, \tag{10}$$

where $\Delta_\pm = 1 \pm \sqrt{1+m^2}$. According to the AdS/CFT correspondence, ρ_{x-} and ρ_{x+} are interpreted as the source and the vacuum expectation value of the vector operator O_x. Besides, μ and S_y correspond to the chemical potential and superfluid velocity, and ρ and J_y are the charge density and current in the dual field theory, respectively. Furthermore, we impose the boundary condition $\rho_{x-} = 0$ since the condensate occurs spontaneously. It is readily to verify that the equations of motion in invariant with respect to the following scaling symmetry of the relevant quantities:

$$\begin{aligned} &r \to \lambda r\,,\ (t,x,y,z) \to \frac{1}{\lambda}(t,x,y,z)\,,\\ &q \to q\,,\ (\rho_x, A_t, A_y) \to \lambda(\rho_x, A_t, A_y)\,,\\ &(T,\mu,S_y) \to \lambda(T,\mu,S_y)\,,\ (\rho, J_y) \to \lambda^3(\rho, J_y)\,,\\ &\rho_{x+} \to \lambda^{1+\Delta_+}\rho_{x+}\,. \end{aligned} \tag{11}$$

We make use of these properties to choose $r_+ = 1$ and $q = 1$ throughout the numerical calculations and present the results in terms of dimensionless quantities.

3 Numerical analysis and results

In this section, we study the effects of the Weyl corrections on the phase transition regarding physical quantities such as superfluid velocity and supercurrent. We explore the relationship between the supercurrent and the superfluid velocity by numerically solving the system of coupled differential eqs. (7)-(9). It is noted that, for the condensed phase with $A_y = 0$, namely, in the absence of the superfluid velocity, the holographic superconductor phase transition is always second order. The result is found to be independent of the Weyl coupling [42]. Furthermore, the critical temperature of the phase transition increases as the coupling increases. This implies that the higher Weyl corrections make it easier for the vector condensate to form. Obviously, this is in contrast to the effects of higher curvature corrections since the latter was shown to hinder the condensate of the vector field [57-59].

By turning on the spatial component A_y, as we will show below, abundant physical contents are unveiled due to the Weyl corrections, regarding the order of phase transition and the phase structure of the model [16,17,20,33,35]. In particular, we evaluate the grand potential $\Omega = -T\mathcal{S}_{\rm os}$ of the dual system in order to investigate the thermodynamical stability of the superconducting as well as normal phase. According to the AdS/CFT correspondence, the grand potential can be evaluated in terms of the Euclidean on-shell action. Moreover, as one is dealing with the grand canonical ensemble, it is possible to evaluate the grand potential as a function of temperature while keeping the chemical potential, among other quantities, unchanged. This can be achieved by making use of the above-mentioned scaling properties in eq. (11). With the help of the equations of motion (4) and (5), one obtains the Euclidean on-shell action $\mathcal{S}_{\rm os}$ as follows:

$$\begin{aligned} \mathcal{S}_{\rm os} =& \int \mathrm{d}^5x\sqrt{-g}\Big\{-\frac{1}{2}\left[\nabla_\mu(A_\nu F^{\mu\nu}) - A_\nu(\nabla_\mu F^{\mu\nu})\right]\\ &+2\gamma[\nabla_\mu(C^{\mu\nu\rho\sigma}A_\nu F_{\rho\sigma}) - A_\nu\nabla_\mu(C^{\mu\nu\rho\sigma}F_{\rho\sigma})]\\ &-[\nabla_\mu(\rho^\dagger_\nu\rho^{\mu\nu}) - \rho^\dagger_\nu(D_\mu\rho^{\mu\nu})] - m^2\rho^\dagger_\mu\rho^\mu\Big\}\\ =& \int \mathrm{d}^5x\sqrt{-g}\Big[-\frac{1}{2}\nabla_\mu(A_\nu F^{\mu\nu}) + 2\gamma\nabla_\mu(C^{\mu\nu\rho\sigma}A_\nu F_{\rho\sigma})\\ &-\nabla_\mu(\rho^\dagger_\nu\rho^{\mu\nu}) + \frac{1}{2}A_\nu\nabla_\mu\left(F^{\mu\nu} - 4\gamma C^{\mu\nu\rho\sigma}F_{\rho\sigma}\right)\Big]\\ =& \frac{V}{T}\Big\{-\frac{1}{2}\sqrt{-h}n_r\left[A_\nu\left(F^{r\nu} - 4\gamma C^{r\nu\rho\sigma}F_{\rho\sigma}\right)\right]|_{r\to\infty}\\ &-\sqrt{-h}n_r\rho^\dagger_\nu\rho^{r\nu}|_{r\to\infty}\\ &+\frac{1}{2}\int_{r_+}^{\infty}\mathrm{d}r\sqrt{-g}A_\nu[\nabla_\mu(F^{\mu\nu} - 4\gamma C^{\mu\nu\rho\sigma}F_{\rho\sigma})]\Big\}, \end{aligned} \tag{12}$$

where we have dropped the prefactor $16\pi G$ of the action (1) for simplicity. Also, the four-volume integration is replaced by $\int \mathrm{d}t\mathrm{d}x\mathrm{d}y\mathrm{d}z = V/T$. By considering that the Weyl term can be neglected near the boundary ($r \to \infty$), we can rewrite the Euclidean on-shell action as:

$$\begin{aligned} \mathcal{S}_{\rm os} =& \frac{V}{T}\Big\{-\frac{1}{2}\sqrt{-h}n_r A_\nu F^{r\nu}|_{r\to\infty} - \sqrt{-h}n_r\rho^\dagger_\nu\rho^{r\nu}|_{r\to\infty}\\ &+\frac{1}{2}\int_{r_+}^{\infty}\mathrm{d}r\sqrt{-g}A_\nu[\nabla_\mu(F^{\mu\nu} - 4\gamma C^{\mu\nu\rho\sigma}F_{\rho\sigma})]\Big\}\\ =& \frac{V}{T}\left[\mu\rho - S_yJ_y + \int_{r_+}^{\infty}\mathrm{d}r\frac{q^2\rho_x^2}{r}\left(A_y^2 - \frac{r^2A_t^2}{f}\right)\right]. \end{aligned} \tag{13}$$

Thus, the grand potential in the superfluid phase reads

$$\frac{\Omega_S}{V} = -\frac{T\mathcal{S}_{\rm os}}{V} = -\mu\rho + S_yJ_y + \int_{r_+}^{\infty}\mathrm{d}r\frac{q^2\rho_x^2}{r}\left(\frac{r^2A_t^2}{f} - A_y^2\right). \tag{14}$$

Apparently, the Weyl coupling parameter γ is absent from eq. (14). However, the Weyl corrections may still affect the grand potential through its influence on the matter fields ρ_x, A_t and A_y. Since $\rho_x = 0$ for the normal phase, in this case, we have $\Omega_N/V = -\mu^2$. In ref. [33], the authors showed that the phase transition in p-wave superfluid model exhibits distinct features for different model parameters. Accordingly, in the following subsections, we will present our results regarding different mass scales of the vector field.

3.1 Small mass scale

Let us first investigate the scenario where the mass of the vector field is small but still beyond the Breitenlohner-Freedman (BF) bound $m^2_{\rm BF} = -1$. Without loss of generality, the numerical results will be mostly focused on the cases where $m^2 = 0$. In Figure 1, we show the calculated condensate

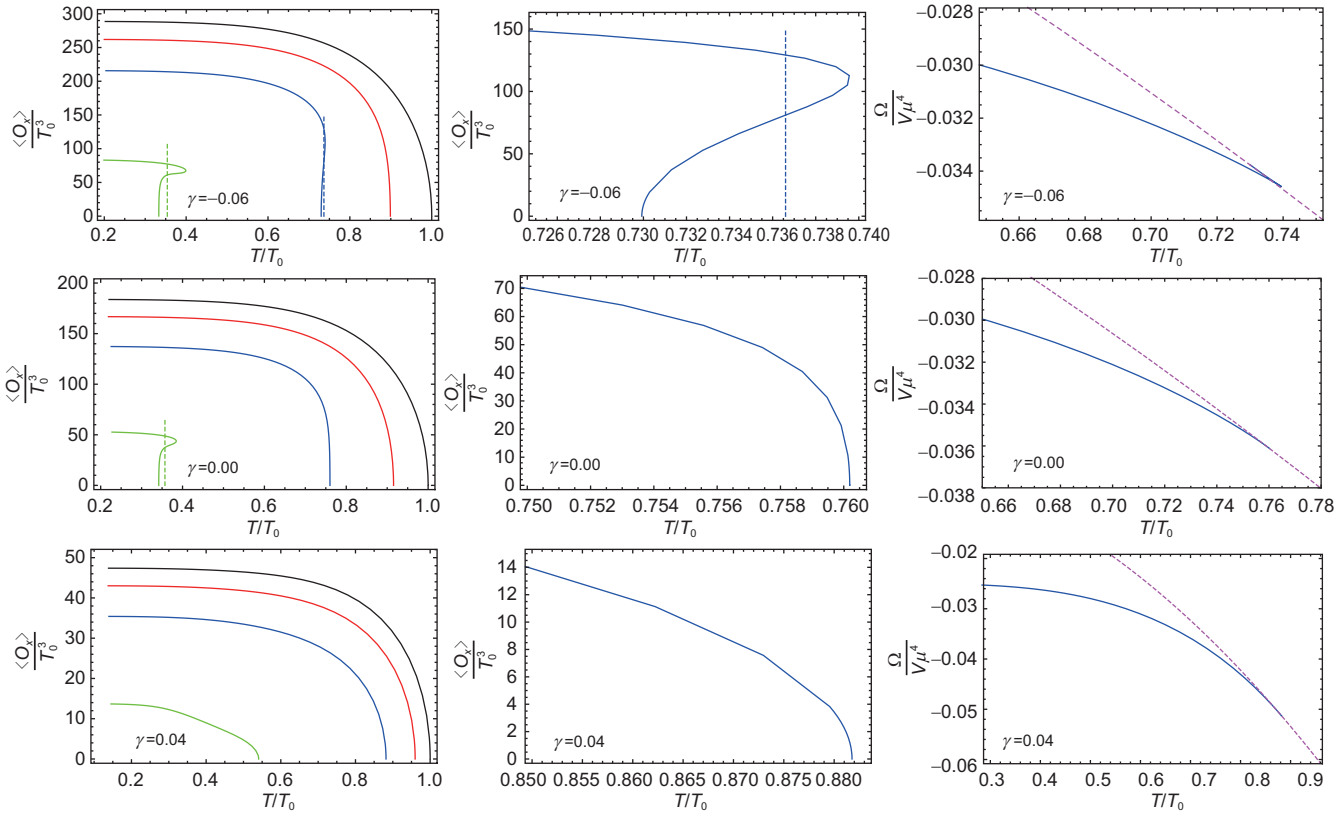

Figure 1 (Color online) The calcualted condensate and grand potential as functions of the temperature for different strength of the Weyl coupling γ. The calculations are carried out for $m^2 = 0$. Left column: the calculated results of condensate for different superfluid velocities $S_y/\mu = 0$ (black), 0.25 (red), 0.42 (blue) and 0.75 (green) increasing to the bottom-left. Middle column: one of the curves shown in the left column, for $S_y/\mu = 0.42$, is zoomed in for the transition region, and in particular, a vertical line has been added to the plots indicating the corresponding critical temperatures of a first-order phase transition determined by the related plots in the right column. Right column: the calculated grand potential of the superfluid phase (blue solid) and the normal phase (magenta dotted), for given superfluid velocity $S_y/\mu = 0.42$.

and grand potential as functions of the temperature for different values of Weyl coupling. As a comparison, we present in the plots the curves for the case $\gamma = 0$ which has been discussed in ref. [33]. The latter corresponds to the usual holographic p-wave superfluid without the Weyl corrections. We adopt the convention used in literature that T_0 is defined as the critical temperature of the transition from the normal phase to the superfluid one at vanishing superfluid velocity $S_y = 0$. When the superfluid velocity is small enough, for example, $S_y/\mu = 0$, 0.25 and $\gamma = -0.06$, one observes that the phase transition from the normal phase to the p-wave superfluid phase is of the second order. In particular, for $S_y = 0$, numerically we find that the critical temperature satisfies the relation $T_0 = 0.0685\mu$ for $\gamma = -0.06$, $T_0 = 0.0796\mu$ for $\gamma = 0.00$, and $T_0 = 0.125\mu$ for $\gamma = 0.04$. In other words, at vanishing superfluid velocity, the critical temperature increases linearly with the chemical potential for given Weyl coupling, while it increases with the Weyl coupling for given chemical potential. The latter indicates that larger Weyl corrections make it easier for the vector condensate to take place. We note that these findings are in contrast to that caused by the higher curvature corrections in the holographic p-wave superfluid model. There, it is shown that more significant curvature corrections make it easier for the phase transition to take place [38].

As the superfluid velocity increases, however, the phase transition is found to evolve to a first-order one. For instance, for $S_y/\mu = 0.42$, 0.75 and $\gamma = -0.06$, the phase transition is of the first order. To better illustrate the results, a dotted vertical line is added to the relevant curves indicating the locations of the temperature where the first-order phase transition occurs. The above assertion can be derived from the calculated grand potential, which is characterized by the typical swallowtail shape as shown by the plots in the right column of Figure 1. Therefore, the order of the phase transition is inferred from Ehrenfest's definition. As a result, there exists a turning point where the second-order phase transition becomes the first order. For instance, for the first row of Figure 1 where $\gamma = -0.06$, the turning point is numerically found to be at $S_y/\mu = 0.317$. In Figure 2, we present a curve formed by connecting all the turning points in the S_y/μ vs. γ plane, for the case $m^2 = 0$. The curve thus defines

the boundary which separates two types of phase transitions. As γ increases, the corresponding S_y/μ essentially increases monotonically. This indicates that for larger Weyl corrections, a more significant superfluid velocity is required for the first-order phase transition to take place. From Figure 2, we find that for some parameter region, the phase transition from the normal phase to the superfluid phase could be of the first order, since the order parameter jumps from zero to a finite value when one increases the superfluid velocity beyond the turning value, just as shown in Figure 1. Such a jump will certainly change the energy and so requires some latent heat, which indicates that the phase transition should be of the first order [23]. This conclusion is consistent with the observation from the curve of the supercurrent J_y vs. the superfluid velocity S_y for a given Weyl coupling γ at a fixed temperature in the following calculations. We also note that Figure 2 shows that the turning point, $S_y/\mu = 0.897$ and $\gamma = 0.04$, locates beyond the range of parameters shown in Figure 1. Therefore, the first-order phase transition cannot be observed among the curves for $\gamma = 0.04$ as shown in Figure 1.

Next, we move to study the relationship between the supercurrent and the superfluid velocity, where the results are presented in Figure 3 for different values of the Weyl coupling. We find that, for all the values of the Weyl coupling γ, the resulting curves are approximately parabolas which open down in accordance with the Ginzburg-Landau model. For a given temperature near T_0, for example $T/T_0 = 0.98$, the maximum value of the supercurrent, denoted by $J_{y\mathrm{Max}}/\mu^3$, is found to decrease with increasing γ. This is similar to the effect caused by the curvature corrections [38]. We also observe that the supercurrent J_y/μ^3 drops sharply and attains zero at $S_{y\mathrm{Max}}/\mu$, namely, the point of intersection between the curve with the axis of abscissas. This implies that the system undergoes a second-order phase transition near the critical temperature T_0, in agreement with thin films of BCS superconductors [60]. For smaller superfluid velocity, it is found that the relation between the supercurrent and the

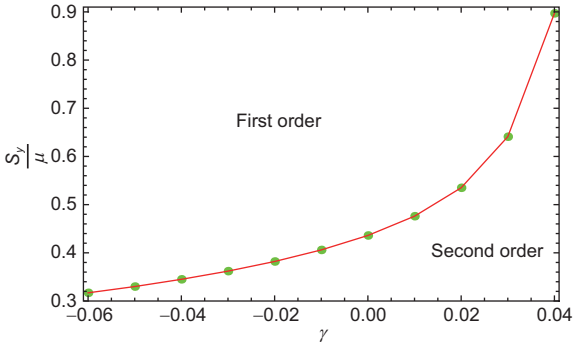

Figure 2 (Color online) The collection of the turning points where the second-order phase transition switches into a first-order one. All the points form a curve in the superfluid velocity S_y/μ vs. the Weyl coupling γ plane. The calculations are carried out for $m^2 = 0$.

superfluid velocity is mostly linear until the maximum $J_{y\mathrm{Max}}/\mu^3$ is reached. For the cases $\gamma = -0.06$ and 0.00, for the region of small temperature and large superfluid velocity in the vicinity of $S_{y\mathrm{Max}}/\mu$, one observes that the supercurrent becomes multivalued as it does not drop to zero monotonically. It is an indication of the latent heat, which subsequently implies the occurrence of a first-order phase transition as discussed earlier regarding Figure 1. On the other hand, for $\gamma = 0.04$, we can see clearly that the holographic superfluid phase transition is always the second order for the range of temperatures considered here. This is in good agreement with the results shown previously in Figures 1 and 2. It should be noted that, the larger the Weyl coupling, the harder it is to find the curve of the supercurrent multivalued. This is, again, in accordance with the above discussions related to Figure 2 and implies that the higher Weyl corrections make it harder for the phase transition to be first order.

On the other hand, as predicted by Ginzburg-Landau theory, the norm of the condensate monotonically decreases with respect to the velocity from its maximum value $\langle O_x\rangle_\infty$ at any fixed temperature, where $\langle O_x\rangle_\infty$ is the value of the condensate corresponding to vanishing superfluid velocity. The norm of the condensate has an intermediate value $\langle O_x\rangle_c$ at the maximum value of the supercurrent $J_{y\mathrm{Max}}/\mu^3$. Thus, Ginzburg-Landau theory predicts

$$\left(\frac{\langle O_x\rangle_c}{\langle O_x\rangle_\infty}\right)^2 = \frac{2}{3}, \tag{15}$$

which shows that the squared ratio of the maximal condensate to the minimal condensate is equal to two-thirds. Since Ginzburg-Landau theory provides an accurate description of various quantities of real physical systems that can be measured experimentally, we will compare our results against eq. (15). In Table 1, we present the calculated ratio $(\langle O_x\rangle_c/\langle O_x\rangle_\infty)^2$ in our holographic p-wave superfluid model for different Weyl corrections. The calculations are carried out for given temperatures and $m^2 = 0$. From Table 1, one observes that, in the vicinity of the critical temperature, the ratio $(\langle O_x\rangle_c/\langle O_x\rangle_\infty)^2$ agrees well with the prediction of Ginzburg-Landau theory independent of the Weyl coupling γ. At lower temperatures, the results gradually deviate from the predicted value.

Table 1 The calculated ratio $(\langle O_x\rangle_c/\langle O_x\rangle_\infty)^2$ for different values of the Weyl coupling γ. The calculations are carried out for given temperature and $m^2 = 0$

T/T_0	$\gamma = -0.06$	$\gamma = 0.00$	$\gamma = 0.04$
0.98	0.664746	0.661292	0.656638
0.7	0.490573	0.508923	0.518068
0.5	0.343464	0.358191	0.419310
0.2	0.304675	0.295584	0.299114

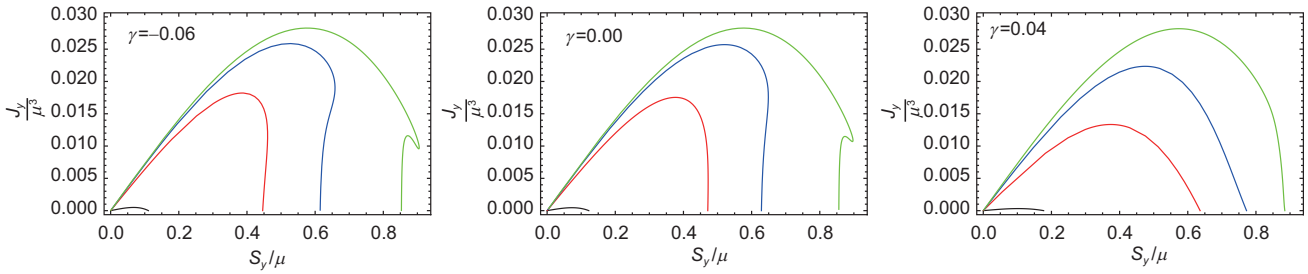

Figure 3 (Color online) The calculated supercurrent as a function of superfluid velocity for different values of the Weyl coupling γ. The calculations are carried out for given temperatures and $m^2 = 0$. In the plots, the four curves correspond to the temperatures $T/T_0 = 0.2$ (green), 0.5 (blue), 0.7 (red) and 0.98 (black) increasing to the bottom-left.

3.2 Intermediate mass scale

In this section, as an illustration, we choose the mass of the vector field to be $m^2 = 5/4$. In Figure 4 we present the calculated condensate and the corresponding grand potential as functions of the temperature for different γ. If the superfluid velocity is small enough, such as $S_y/\mu = 0$ and 0.50 with $\gamma = -0.06$, the phase transition is found to be of the second order. Meanwhile, near the critial temperature the condensate satisfies scaling $\langle O_x \rangle \sim (T_c - T)^{1/2}$ for all values of γ. On the other hand, for large superfluid velocity, interesting enough, the vector operator O_x becomes multivalued for given temperatures and the Cave of Winds feature appears [20, 34]. This happens, for example for $S_y/\mu = 0.70$ and 0.80 with $\gamma = -0.06$. As discussed above, by examing the evaluated grand potential, one can retrieve information on which phase is thermodynamically favored as well as the order of the phase transition. In other words, the properties of the phase transition can be extracted by studying the Cave of Winds shown by the plots in the right column of Figure 4. For a given superfluid velocity, $S_y/\mu = 0.70$, one finds that the phase transition is of the second order for $\gamma = 0.04$. The Cave of Winds starts to appear as γ decreases, as shown in the plots, for $\gamma = 0.00$ and -0.06, a second superfluid phase emerges, and the transition between the two superfluid phases is of the first order. On the other hand, the transition from the normal phase to a superfluid phase remains to be second order. Therefore, one concludes that for larger Weyl corrections, it becomes more difficult for the Cave of Winds to appear, as it requires more substantial superfluid velocity. We note that this result is in contrast with the effect of higher curvature corrections. The latter is found to facilitate the emergence of the Cave of Winds [38]. Regarding the relationship between critical temperature and Weyl coupling, we focus on the case where $S_y = 0$. From Figure 4, it is found that $T_0 = 0.0523\mu$ for $\gamma = -0.06$, $T_0 = 0.0614\mu$ for $\gamma = 0.00$, and $T_0 = 0.101\mu$ for $\gamma = 0.04$. Thus one concludes that the critical temperature increases as the Weyl coupling γ increases. In this context, larger Weyl correction promotes the transition to the p-wave superfluid phase from the normal phase, by raising the corresponding critical temperature.

In Figure 5, we show the supercurrent as a function of the superfluid velocity for different values of the Weyl coupling γ. The calculations are done by assuming $m^2 = 5/4$. We notice that, near the critical temperature, for instance, $T/T_0 = 0.98$, the curve of the supercurrent vs the superfluid velocity is approximately a parabola opening down. The phase transition is found to be second order. This result is similar to the previous case of $m^2 = 0$. As the temperature decreases to a specific value, approximately at $T/T_0 = 0.20$ as shown in the plots for $\gamma = -0.06$ and 0.00, the second-order phase transition turns into a first-order one. Meanwhile, the critical temperature increases as the Weyl coupling increases, reinforcing the above findings in Figure 4 that larger Weyl corrections make it harder for the emergence of the Cave of Winds.

In Table 2, we present the results on the ratio $(\langle O_x \rangle_c / \langle O_x \rangle_\infty)^2$ for different Weyl coupling γ. The calculations are done for given temperatures and $m^2 = 5/4$. It is found that, in the vicinity of the critical temperature, for example, $T/T_0 = 0.98$, the ratio is in good agreement with the value 2/3 predicted in Ginzburg-Landau theory. It is also observed that the ratio deviates more significantly from the above value as the temperature decreases further.

3.3 Large mass scale

Without loss of generality, to study the case of the relatively large mass for the vector field, we take $m^2 = 3$ in the following calculations. The resultant condensate and grand potential as functions of temperature for different values of γ are shown in Figure 6. We note that for the present case, the

Table 2 The calculated ratio $(\langle O_x \rangle_c / \langle O_x \rangle_\infty)^2$ for different Weyl coupling γ. The calculations are carried out for given temperature and $m^2 = 5/4$

T/T_0	$\gamma = -0.06$	$\gamma = 0.00$	$\gamma = 0.04$
0.98	0.662083	0.661859	0.654922
0.7	0.486774	0.488186	0.494584
0.5	0.302286	0.315156	0.373089
0.2	0.243731	0.245285	0.247934

role of $\frac{q^2A_y^2}{r^2}$ becomes insignificant and therefore can be safely ignored from eq. (7). The phase transition is found to be always of the second order, while the Weyl corrections do not qualitatively alter this result, independent of the magnitude of superfluid velocity. This result agrees with what can be inferred from the calculated grand potential shown in the right column of Figure 6. Moreover, we find that the critical temperatures T_0 for vanishing superfluid velocity $S_y = 0$ satisfies $T_0 = 0.0421\mu$ for $\gamma = -0.06$, $T_0 = 0.0498\mu$ for $\gamma = 0.00$, and $T_0 = 0.0851\mu$ for $\gamma = 0.04$. It is observed that the critical temperature increases with increasing Weyl coupling, which indicates that higher Weyl corrections make it easier for the condensate to form, for the present case of large mass scale.

In Figure 7, the calculated supercurrent is presented as a function of superfluid velocity. The resulting curves are approximately parabolas opening down, and in particular, they mostly decrease monotonically near $S_{y\mathrm{Max}}/\mu$. Therefore, the corresponding holographic superfluid phase transition is of the second order for the temperatures considered. We also point out that the Weyl correction cannot change the order of

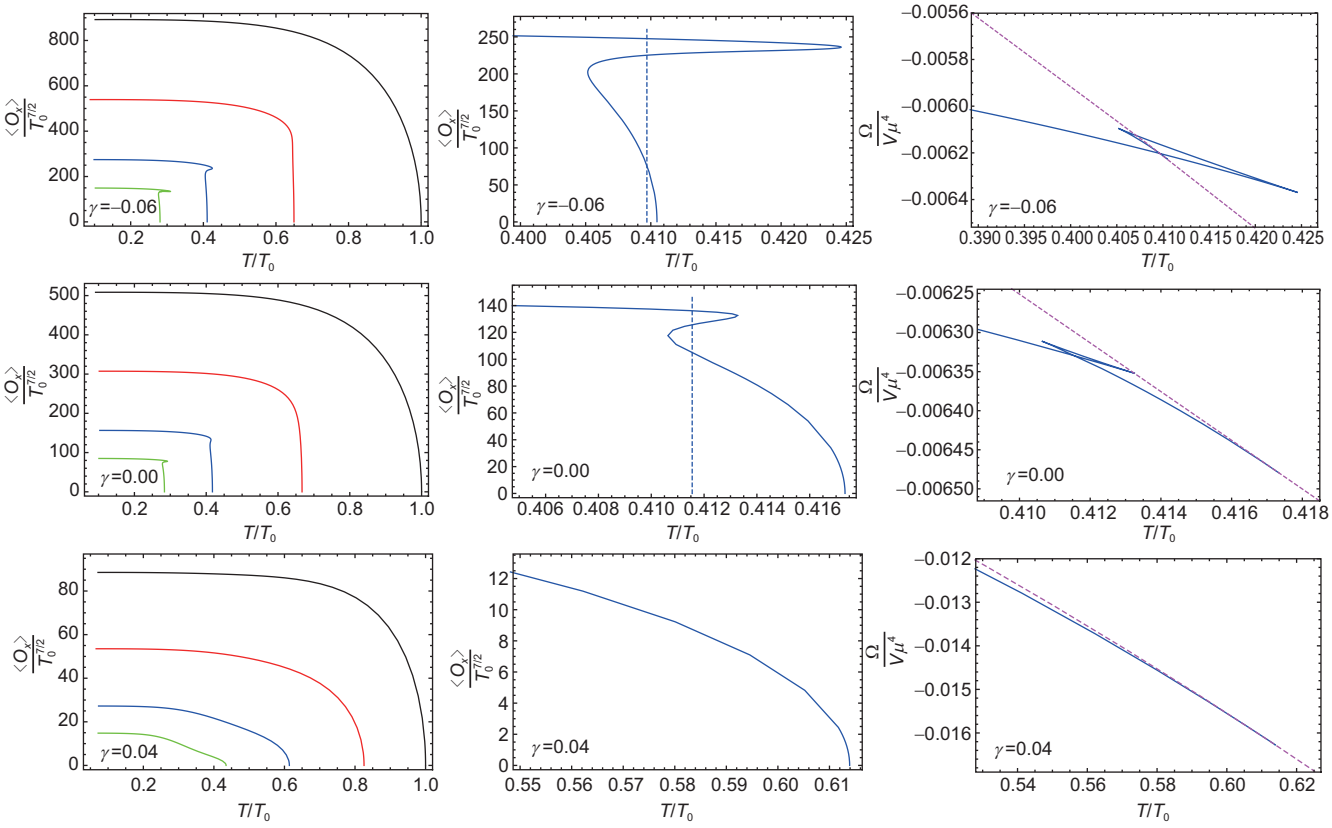

Figure 4 (Color online) The calculated condensate and grand potential as functions of the temperature for different values of the Weyl coupling γ. The calculations are carried out for $m^2 = 5/4$. Left column: the calculated results of condensate for different superfluid velocities $S_y/\mu = 0$ (black), 0.50 (red), 0.70 (blue) and 0.80 (green) increasing to the bottom-left. Middle column: one of the curves shown in the left column, for $S_y/\mu = 0.70$, is zoomed in for the transition region, and in particular, a vertical line has been added to the plots indicating the corresponding critical temperature where a first-order phase transition takes place. The critical temperature of the transition is determined by the related plot in the right column. Right column: the calculated grand potential of the superfluid phase (blue solid) and the normal phase (magenta dotted), for given superfluid velocity $S_y/\mu = 0.70$.

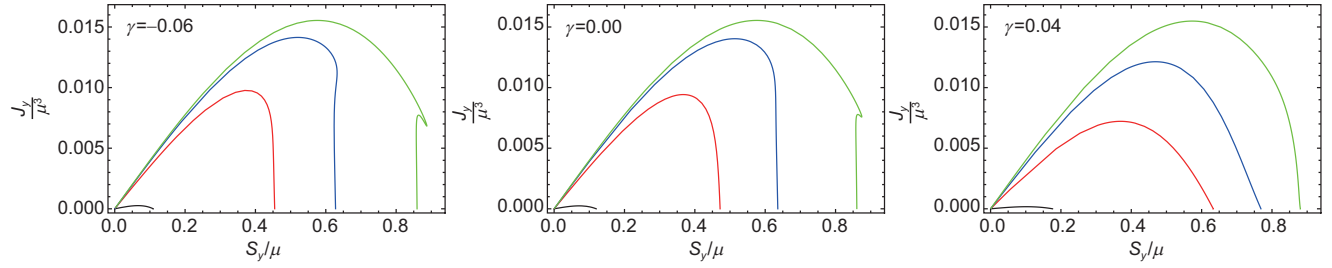

Figure 5 (Color online) The calculated supercurrent as a function of superfluid velocity for different values of the Weyl coupling γ. The calculations are carried out for given temperatures and $m^2 = 5/4$. In the plots, the four curves correspond to the temperatures $T/T_0 = 0.2$ (green), 0.5 (blue), 0.7 (red) and 0.98 (black) increasing to the bottom-left.

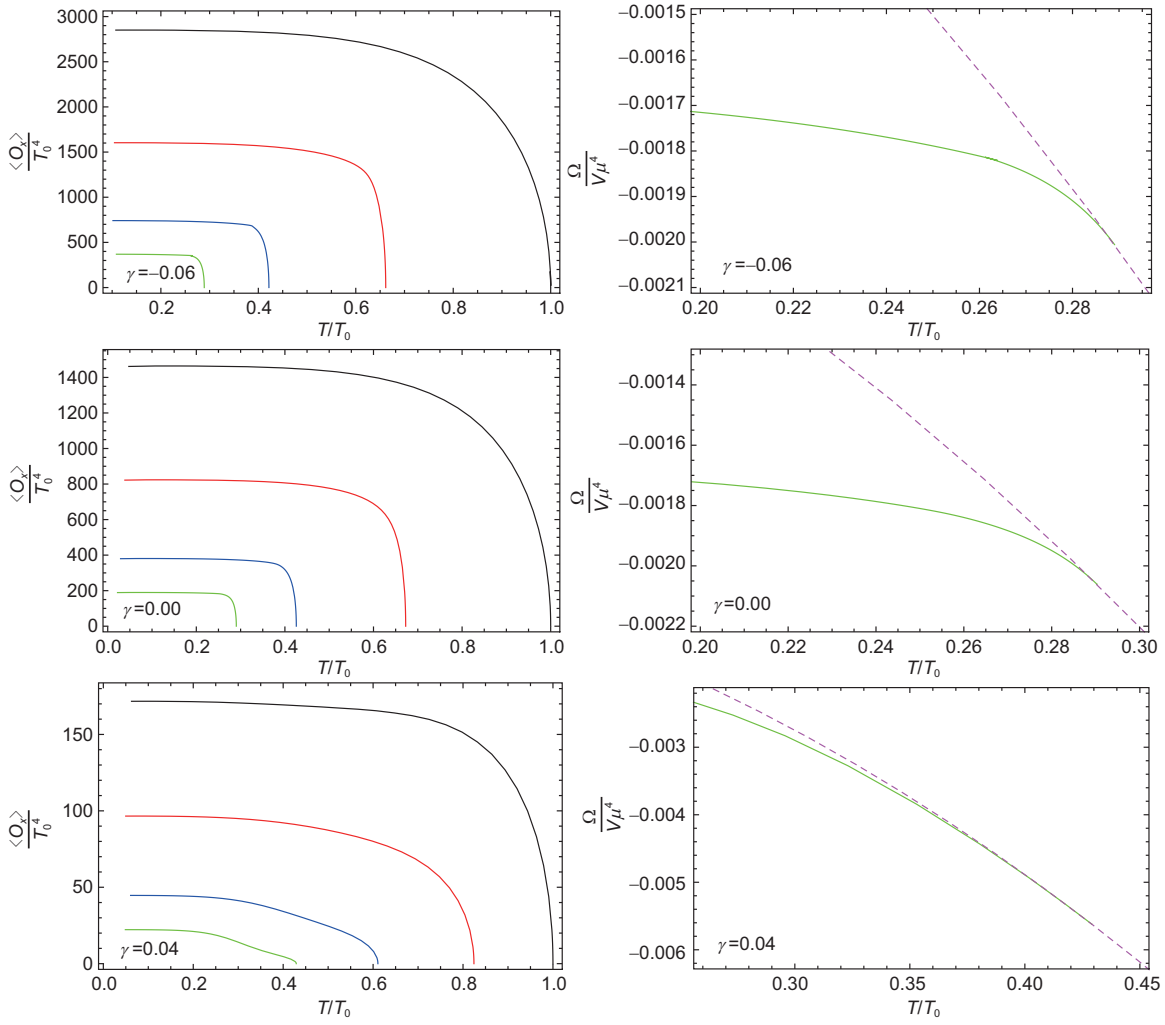

Figure 6 (Color online) The calcualted condensate and grand potential as functions of the temperature for different strength of the Weyl coupling γ. The calculations are carried out for $m^2 = 3$. Left column: the calculated results of condensate for different superfluid velocities $S_y/\mu = 0$ (black), 0.5 (red), 0.7 (blue) and 0.8 (green) increasing to the bottom-left. Right column: the calculated grand potential of the superfluid phase (blue solid) and the normal phase (magenta dotted), for given superfluid velocity $S_y/\mu = 0.8$.

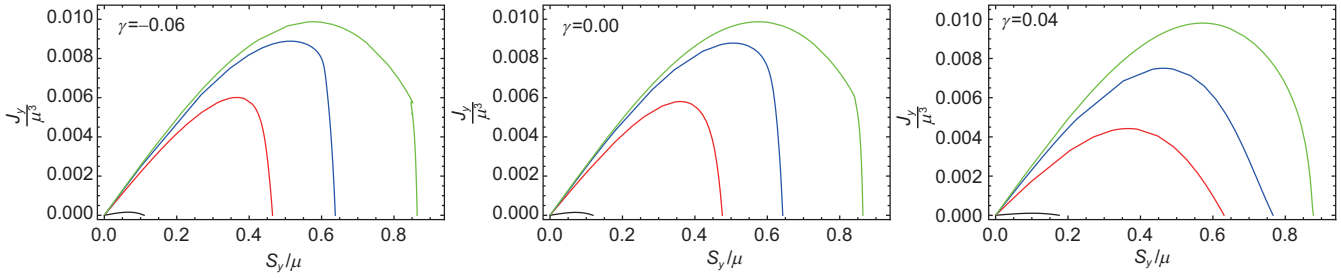

Figure 7 (Color online) The calculated supercurrent as a function of superfluid velocity for different values of the Weyl coupling γ. The calculations are carried out for given temperatures and $m^2 = 3$. In the plots, the four curves correspond to the temperatures $T/T_0 = 0.2$ (green), 0.5 (blue), 0.7 (red) and 0.98 (black) increasing to the bottom-left.

phase transition in the present case, consistent with discussions regarding Figure 6.

In Table 3, we present the ratio $(\langle O_x \rangle_c / \langle O_x \rangle_\infty)^2$ for different values of γ with given temperature. It is found that, near the critical temperature, such as $T/T_0 = 0.98$, the calculated ratio is numerically consistent with $2/3$ that predicted by Ginzburg-Landau theory. This behavior is reminiscent of what has been observed in the cases of $m^2 = 0$ and $5/4$. Regarding the ratio of condensate with vanishing superfluid velocity to that with maximal superfluid velocity, the present model is in good agreement with Ginzburg-Landau theory in the vicinity of the critical temperature. This conclusion is

Table 3 The calculated ratio $(\langle O_x\rangle_c/\langle O_x\rangle_\infty)^2$ for different Weyl coupling γ. The calculations are carried out for given temperature and $m^2 = 3$

T/T_0	$\gamma = -0.06$	$\gamma = 0.00$	$\gamma = 0.04$
0.98	0.665338	0.662788	0.652647
0.7	0.455204	0.477465	0.461653
0.5	0.257971	0.283605	0.338367
0.2	0.196161	0.198243	0.198158

valid regardless of the strength of the Weyl coupling or the mass of the vector field.

4 Concluding remarks

In this work, we have constructed a holographic p-wave superfluid model with Weyl corrections. In the probe limit, the condensate of a complex vector field is analyzed, in order to understand the influences of the $1/N$ or $1/\lambda$ corrections on the superfluid phase transition systematically. We compared the effects of the Weyl corrections against those of the higher order curvature corrections [38]. Although both are associated with higher order derivatives of the metric, it is found that those two types of corrections lead to significant differences. In particular, in contrast to the effect of curvature corrections, the critical temperature increases with the Weyl coupling regardless of the superfluid velocity or the mass of the vector field. This implies that the Weyl corrections make it easier for the p-wave superfluid phase transition to be triggered. Also, analyses were carried out regarding the different mass scales of the vector field. While considering the case of a small mass scale, we observed that larger Weyl coupling results in larger superfluid velocity for the turning point, where the transition switches from the second order to the first order. In the case of intermediate mass scale, it was shown that the larger Weyl corrections hinder the appearance of a feature in the phase structure of the system, known as Cave of Winds. By comparing with the curvature corrections in the holographic p-wave superfluid model, we found that the effects on the emergence of Cave of Winds from these two corrections are opposite. For a large mass scale, numerical studies showed that the phase transition of the system is always of the second order, independent of the strength of the Weyl corrections. Moreover, conclusions drawn from the relation between the supercurrent and the superfluid velocity agree with those obtained from the condensate of the vector field. In particular, in the vicinity of the critical temperature, we observed that the ratio $(\langle O_x\rangle_c/\langle O_x\rangle_\infty)^2 \simeq 2/3$ is numerically consistent with that predicted by Ginzburg-Landau theory. Weyl correction considered in the present study does not modify this relation for $T \sim T_0$. Although the present approach captures the essential features of the phase structure, it would be interesting to extend the discussions beyond the probe limit. We plan to investigate the topic in the future further.

This work was supported by the National Natural Science Foundation of China (Grant Nos. 11775076, 11875025, 11475061, and 11690034), Hunan Provincial Natural Science Foundation of China (Grant No. 2016JJ1012), Brazilian funding agencies Fundação de Amparo à Pesquisa do Estado de São Paulo (FAPESP), Conselho Nacional de Desenvolvimento Científico e Tecnológico (CNPq), and Coordenação de Aperfeiçoamento de Pessoal de Nível Superior (CAPES).

1 J. G. Bednorz, and K. A. Müller, Z. Phys. B-Condensed Matt. **64**, 189 (1986).
2 J. Bardeen, L. N. Cooper, and J. R. Schrieffer, Phys. Rev. **108**, 1175 (1957).
3 J. Maldacena, Adv. Theor. Math. Phys. **2**, 231 (1998); Int. J. Theor. Phys. **38**, 1113 (1999).
4 S. S. Gubser, I. R. Klebanov, and A. M. Polyakov, Phys. Lett. B **428**, 105 (1998).
5 E. Witten, Adv. Theor. Math. Phys. **2**, 253 (1998).
6 S. A. Hartnoll, C. P. Herzog, and G. T. Horowitz, J. High Energy Phys. **12**, 15 (2008), arXiv: 0810.1563.
7 S. S. Gubser, Phys. Rev. D **78**, 065034 (2008), arXiv: 0801.2977.
8 S. A. Hartnoll, C. P. Herzog, and G. T. Horowitz, Phys. Rev. Lett. **101**, 031601 (2008), arXiv: 0803.3295.
9 S. A. Hartnoll, Class. Quantum Grav. **26**, 224002 (2009), arXiv: 0903.3246.
10 C. P. Herzog, J. Phys. A-Math. Theor. **42**, 343001 (2009), arXiv: 0904.1975.
11 G. T. Horowitz, Lect. Notes Phys. **828**, 313 (2011).
12 R. G. Cai, L. Li, L. F. Li, and R. Q. Yang, Sci. China-Phys. Mech. Astron. **58**, 060401 (2015), arXiv: 1502.00437.
13 S. S. Gubser, and S. S. Pufu, J. High Energy Phys. **11**, 33 (2008), arXiv: 0805.2960.
14 J. W. Chen, Y. J. Kao, D. Maity, W. Y. Wen, and C. P. Yeh, Phys. Rev. D **81**, 106008 (2010), arXiv: 1003.2991.
15 F. Benini, C. P. Herzog, R. Rahman, and A. Yarom, J. High Energ. Phys. **11**, 137 (2010), arXiv: 1007.1981.
16 P. Basu, A. Mukherjee, and H. H. Shieh, Phys. Rev. D **79**, 045010 (2009).
17 C. P. Herzog, P. K. Kovtun, and D. T. Son, Phys. Rev. D **79**, 066002 (2009), arXiv: 0809.4870.
18 Y. Peng, X. M. Kuang, Y. Q. Liu, and B. Wang, arXiv: 1204.2853.
19 X. M. Kuang, Y. Liu, and B. Wang, Phys. Rev. D **86**, 046008 (2012), arXiv: 1204.1787.
20 D. Arean, P. Basu, and C. Krishnan, J. High Energ. Phys. **10**, 6 (2010), arXiv: 1006.5165.
21 D. D. Arean, M. Bertolini, J. Evslin, and T. Prochazka, J. High Energ. Phys. **7**, 60 (2010), arXiv: 1003.5661.
22 J. Sonner, and B. Withers, Phys. Rev. D **82**, 026001 (2010), arXiv: 1004.2707.
23 H. B. Zeng, W. M. Sun, and H. S. Zong, Phys. Rev. D **83**, 046010 (2011), arXiv: 1010.5039.
24 I. Amado, D. Arean, A. Jimenez-Alba, K. Landsteiner, L. Melgar, and I. S. Landea, J. High Energ. Phys. **7**, 108 (2013).
25 H. B. Zeng, Phys. Rev. D **87**, 046009 (2013), arXiv: 1204.5325.
26 I. Amado, D. Arean, A. Jimenez-Alba, K. Landsteiner, L. Melgar, and I. S. Landea, J. High Energ. Phys. **2**, 63 (2014), arXiv: 1307.8100.
27 R. E. Arias, and I. S. Landea, Phys. Rev. D **94**, 126012 (2016), arXiv: 1608.01687.
28 R. G. Cai, S. He, L. Li, and L. F. Li, J. High Energ. Phys. **12**, 36 (2013), arXiv: 1309.2098.

29 R. G. Cai, L. Li, and L. F. Li, J. High Energ. Phys. **1**, 32 (2014), arXiv: 1309.4877.
30 L. F. Li, R. G. Cai, L. Li, and C. Shen, Nucl. Phys. B **894**, 15 (2015), arXiv: 1310.6239.
31 R. G. Cai, L. Li, L. F. Li, and R. Q. Yang, J. High Energ. Phys. **4**, 16 (2014), arXiv: 1401.3974.
32 Z. Y. Nie, Q. Pan, H. B. Zeng, and H. Zeng, Eur. Phys. J. C **77**, 69 (2017), arXiv: 1611.07278.
33 Y. B. Wu, J. W. Lu, W. X. Zhang, C. Y. Zhang, J. B. Lu, and F. Yu, Phys. Rev. D **90**, 126006 (2014), arXiv: 1410.5243.
34 M. Sun, D. Wang, Q. Pan, and J. Jing, Eur. Phys. J. C **79**, 145 (2019), arXiv: 1812.00649.
35 Y. B. Wu, J. W. Lu, C. Y. Zhang, N. Zhang, X. Zhang, Z. Q. Yang, and S. Y. Wu, Phys. Lett. B **741**, 138 (2015), arXiv: 1412.3689.
36 C. Lai, Q. Pan, J. Jing, and Y. Wang, Phys. Lett. B **757**, 65 (2016), arXiv: 1601.00134.
37 M. Rogatko, and K. I. Wysokinski, J. High Energ. Phys. **10**, 152 (2016), arXiv: 1608.00343.
38 S. Liu, Q. Pan, and J. Jing, Phys. Lett. B **765**, 91 (2017), arXiv: 1610.02549.
39 A. Ritz, and J. Ward, Phys. Rev. D **79**, 066003 (2009), arXiv: 0811.4195.
40 S. Chen, and J. Jing, Phys. Rev. D **88**, 064058 (2013), arXiv: 1307.7459; Phys. Rev. D **89**, 104014 (2014), arXiv: 1310.1807; Phys. Rev. D **90**, 124059 (2014), arXiv: 1408.5324.
41 J. P. Wu, Y. Cao, X. M. Kuang, and W. J. Li, Phys. Lett. B **697**, 153 (2011), arXiv: 1010.1929.
42 L. Zhang, Q. Pan, and J. Jing, Phys. Lett. B **743**, 104 (2015), arXiv: 1502.05635.
43 D. Z. Ma, Y. Cao, and J. P. Wu, Phys. Lett. B **704**, 604 (2011), arXiv: 1201.2486.
44 D. Momeni, and M. R. Setare, Mod. Phys. Lett. A **26**, 2889 (2011), arXiv: 1106.0431.
45 D. Momeni, N. Majd, and R. Myrzakulov, Europhys. Lett. **97**, 61001 (2012), arXiv: 1204.1246.
46 D. Roychowdhury, Phys. Rev. D **86**, 106009 (2012),
47 D. Momeni, M. R. Setare, and R. Myrzakulov, Int. J. Mod. Phys. A **27**, 1250128 (2012), arXiv: 1209.3104.
48 Z. Zhao, Q. Pan, and J. Jing, Phys. Lett. B **719**, 440 (2013), arXiv: 1212.3062.
49 D. Momeni, R. Myrzakulov, and M. Raza, Int. J. Mod. Phys. A **28**, 1350096 (2013), arXiv: 1307.8348.
50 L. Zhang, H. Li, H. Zhao, and R. Zhao, Int. J. Theor. Phys. **52**, 2455 (2013).
51 S. A. H. Mansoori, B. Mirza, A. Mokhtari, F. L. Dezaki, and Z. Sherkatghanad, J. High Energ. Phys. **7**, 111 (2016), arXiv: 1602.07245.
52 D. Momeni, M. Raza, and R. Myrzakulov, Int. J. Geom. Methods Mod. Phys. **13**, 1550131 (2016), arXiv: 1410.8379.
53 Y. Ling, P. Liu, J. P. Wu, and Z. Zhou, Phys. Lett. B **766**, 41 (2017), arXiv: 1606.07866.
54 G. Fu, J. P. Wu, B. Xu, and J. Liu, Phys. Lett. B **769**, 569 (2017), arXiv: 1705.06672.
55 Y. Ling, and X. Zheng, Nucl. Phys. B **917**, 1 (2017), arXiv: 1609.09717.
56 J. P. Wu, and P. Liu, Phys. Lett. B **774**, 527 (2017). arXiv: 1710.07971; Phys. Lett. B **780**, 616 (2018), arXiv: 1804.10897.
57 J. W. Lu, Y. B. Wu, T. Cai, H. M. Liu, Y. S. Ren, and M. L. Liu, Nucl. Phys. B **903**, 360 (2016).
58 R. G. Cai, Z. Y. Nie, and H. Q. Zhang, Phys. Rev. D **82**, 066007 (2010), arXiv: 1007.3321.
59 Z. Y. Nie, and H. Zeng, J. High Energ. Phys. **2015(10)**, 47 (2015), arXiv: 1505.02289.
60 M. Tinkham, *Introduction to Superconductivity* (McGrawHill, New York, 1996).